IEEE Access
Multidisciplinary | Rapid Review | Open Access Journal

Received July 14, 2018, accepted August 9, 2018, date of publication August 16, 2018, date of current version September 7, 2018.

Digital Object Identifier 10.1109/ACCESS.2018.2865807

Design and Information Architectures for an Unmanned Aerial Vehicle Cooperative Formation Tracking Controller

JIALONG ZHANG[1], (Student Member, IEEE), JIANGUO YAN[1], PU ZHANG[1], AND XIANGJIE KONG[2], (Senior Member, IEEE)

[1]School of Automation, Northwestern Polytechnical University, Xi'an 710129, China
[2]Key Laboratory for Ubiquitous Network and Service Software of Liaoning Province, School of Software, Dalian University of Technology, Dalian 116620, China

Corresponding authors: Jialong Zhang (zjl0117@mail.nwpu.edu.cn) and Xiangjie Kong (xjkong@ieee.org)

This work was supported by the National Natural Science Foundation of China under Grant 60974146 and Grant 61473229.

ABSTRACT This paper addresses a well-documented open problem on the tracking target of the multiple unmanned aerial vehicles (UAVs) subject to the inconsistent of attitude and position in the process of flight. The main contribution is to study a UAV cooperative formation control of tracking a moving target and analyze the flight stability of the designed controller when only knowing the UAV local information. The path planning of a single UAV and multiple UAV cooperative formation tracking of a moving target is studied. First, the feedback control is used to ensure heading convergence for the path planning of a single UAV. Furthermore, we use a variable airspeed controller to achieve the desired angular spacing and build the information architecture using graph theory for the UAV formation tracking of moving targets. The communication data management module at the cloud stores and transmits to UAV by the ground station. The ground command can maintain a UAV control center which gets access to the cloud for the UAV activity management. In addition, the design of a distributed control law is achieved based on the type of information construction between UAVs. The simulation results show that the designed controller is robust for tracking moving targets and achieves good flight-stability when tracking such targets.

INDEX TERMS Collision avoidance, information architecture, cloud-based UAV formation, path planning, flight-stability.

I. INTRODUCTION

Recently, multi-agent formation control has seen great achievements. For formations of small UAVs, each UAV is equipped with sensing, communication, computation and control systems [1], which can provide distributed measurements of distance, displacements and angle spacing from other UAVs. Moreover, these data collections and transmissions are critical aspects for the UAV-based internet of things (IoT) services [2]. However, the concept of the design of large UAVs has been extended to complex Multi-UAV formations. The mission implementation ability of a single UAV is limited. For Multi-UAV formations, control, communication, perception, and computer processing of dates [3]–[11] must be completed by distributed control strategies, which presents higher requirements on Multi-UAV formation.

At present, the issue of Multi-UAV cooperative formation control has been studied. Multi-UAV system is typical multi-agent system. An agent can measure the relative distance from an adjacent agent and control the displacement to achieve the desired formation. However, they do not directly control the relative positions between them because they do not have the same sense of orientation. There have also been a large number of studies on UAV cooperative formation control [12], [13], therein providing path planning, optimal perceptual geometry, distributed control law design, and information architectures. This paper mainly studies two key aspects: the distributed control law design and an extended information architecture. Moreover, we illustrate their convergence via the cooperative tracking problem.

In practical engineering, collision avoidance control algorithms have been applied to real-world UAV formations by many researchers. Nie *et al.* [12] considered a collision avoidance problem between two aircrafts in a three-dimensional environment using a combination of

a geometric approach and a collision-cone approach, and they proposed a guidance law based on the collision-cone approach Cetin and Yilmaz [13] proposed a vision-based collision avoidance system for a single UAV using a single sensor. Bullo [14] performed a feasibility study for a collision avoidance algorithm compatible with the Traffic Alert and Collision Avoidance System used for manned aircraft. Abu-Jbara *et al.* [15] presented a fully autonomous multi-sensor anti-collision system for UAVs with collision geometry with the purpose of detecting and avoiding obstacles and generating feasible trajectories in real time.

As we all know, the important use of UAV formation is to detect and track moving targets. A UAV formation can be used to engage and assess unknown or adversarial targets to provide reconnaissance or detect potential threats in a surrounding environment, thereby playing a guard role in many respects. In cooperative tracking for UAV formations, the Multi-UAVs only use local information to fly in a circular orbit around a moving obstacle with a predetermined angular spacing. When a given target's attitude and position information are known, the UAVs can distribute themselves around the target with an optimal geometry at equal angles [14]. In recent years, Abu-Jbara *et al.* [15] proposed a Lyapunov guidance vector field method to maintain a prescribed tracking radius. Their studies neglected an important timescale separation issue, including heading and radius convergence. For the tracking problem, Kingston and Beard also used a Lyapunov guidance vector field approach to the tracking problem and only used the heading to obtain the desired circular orbit and spatial position [16]. However, they neglected the timescale separation issue when using a dynamic sliding mode controller to ensure the heading converged in finite time. They also used the symmetrical information structure of the UAV formation to increase the number of UAVs and provide some flight-stability results.

Hence, based on the deficiencies in the studies by the above scholars, we further study the Lyapunov guidance vector field approach to fly in the desired circular orbit. The main contributions of this study, relative to other works, are as follows:

1) We propose a heading convergence method by addressing the time-scale separation problem, which takes advantage of the guidance field.
2) To keep the UAV formation flying in a circular orbit, we use a variable airspeed controller to control the UAV formation.
3) We can solve the UAV formation cooperative tracking problem with rigid graph theory, while we use two types of information architectures, including symmetrical and asymmetric structures. We then use them to design the decentralized control law. These information architectures can be extended to Multi-UAVs. Moreover, the designed control law is distributed using only local information.

In this paper, the simulation results present three novel features: (1) the satisfaction of the specific constraints on the UAV heading rate and variable airspeed, (2) the variable airspeed controller being able to achieve the UAV cooperative formation flight with the prescribed angular spacing, and (3) the establishment of information flow between any two UAVs using rigid graph theory. Specifically, we build the information architecture using a graph $G(V, E)$, where V is a point set, indicating a single UAV, and E is an edge set, indicating the flow of information between any two UAVs [17].

The rest of this paper is organized as: In Section II, the UAV dynamics model and the Lyapunov guidance field approach are proposed. In Section III, we apply the above results to the situation with a moving target and wind (with a velocity that is not constant). Adaptive estimates are applied to a situation with wind and non-accelerating moving targets to achieve the desired circular orbit and angular spacing. In Section IV, we briefly review previous work on the concept of graph theory to provide meaningful information architectures for UAV formations toward achieving the decentralized control law design. In Section V, we propose a variable airspeed control law and use two different information architectures to achieve the desired angular spacing. Finally, the concluding remarks are stated in Section VI.

II. THE UAV MODEL

This section establishes the kinematic model of a single UAV in the desired circle orbit and presents a Lyapunov guidance vector field method. We first study the kinematic characteristics of a single UAV in the no-wind, stationary target case and then generalize these results to unknown wind conditions and moving targets.

A. ESTABLISHING LYAPUNOV VECTOR FIELD CONSTRUCTION

The kinematic model of a single fixed-wing UAV with kinematic constraints is as follows [18]:

$$\begin{cases} \dot{x} = \mu_1 \cos\psi \\ \dot{y} = \mu_1 \sin\psi \\ \dot{\psi} = \mu_2 \end{cases} \tag{1}$$

where $[x, y]^T \in R^2$ is the position in the UAV's inertial coordinates, ψ is the heading angle, μ_1 is the command of the airspeed, and μ_2 is the command of the heading. This is a simplification of a real UAV. It is known that a UAV can maintain stability in the vertical direction. However, the model analysis of a UAV is more complicated in the horizontal plane, and the input dynamics with second-order control are easily ignored. Moreover, a single UAV was studied in both the horizontal plane and the vertical direction, which is also a comprehensive description of UAV motion in the literature [15], [19]–[20]. It has important significance for applying dynamic constraints to the model in the actual project. Suppose that there are constraints on the maximum and minimum airspeed based on inequation (2):

$$0 < \upsilon_{\min} \leq \mu_1 \leq \upsilon_{\max} \tag{2}$$

Then, the heading angular rate constraint is based on inequation (3):

$$|\mu_2| \leq \omega_{\max} \tag{3}$$

The maximum heading angular rate constraint is equivalent to a minimum turning radius constraint, where $r_{\min} = 4\mu_1/\omega_{\max}$ [18], the heading angular and airspeed commands are generated from a Lyapunov vector field that guides the UAV in a circular orbit around the target, while the target is stationary. Consider the Lyapunov function [1], as shown in equation (4):

$$V(r) = \frac{1}{2}\left(r^2 + r_d^2\right)^2 \tag{4}$$

Here, $r = \sqrt{x^2 + y^2}$ is the relative distance between the UAV and the target, and r_d is the desired circular tracking orbit radius. To achieve the motion of the UAV in a circular orbit, we choose the desired inertia velocity based on the vector field. Its vector field is as follows:

$$f(x, y) = \begin{bmatrix} \dot{x} \\ \dot{y} \end{bmatrix} = -\frac{\mu_o}{r\left(r^2 + r_d^2\right)} \begin{bmatrix} x\left(r^2 - r_d^2\right) + y\left(2rr_d\right) \\ y\left(r^2 - r_d^2\right) - x\left(2rr_d\right) \end{bmatrix} \tag{5}$$

Here, μ_0 is the relative airspeed of the UAV in the inertial frame and $r \neq 0$. The guidance vector field is expressed in polar coordinates, as shown in Eq. (6):

$$g(r, \theta) = \begin{bmatrix} \dot{r} \\ r\dot{\theta} \end{bmatrix} = \frac{\mu_0}{r^2 + r_d^2} \begin{bmatrix} -\left(r^2 - r_d^2\right) \\ 2rr_d \end{bmatrix} \tag{6}$$

Qualitative analysis shows that when $r > r_d$, r decreases toward the desired circular orbit radius; when $r < r_d$, r increases away from the desired circular orbit radius; and when $r = r_d$, r is the desired circular orbit radius with a constant angular speed of $\dot{\theta} = \mu_0/r_d$, which is an ideal case. We calculate these trajectories using the derivative of Eq. (4), as shown in the following equation:

$$\dot{V} = -\frac{4\mu_0 r\left(r^2 - r_d^2\right)^2}{r^2 + r_d^2} \leq 0 \tag{7}$$

According to LaSalle's principle of invariance, the trajectory of the UAV converges asymptotically to the desired orbit radius [15]. The vector field is obtained an approximate analytical method. Observe that the kinematics Eq. 6 is independent of θ, and Eq. (8) can be obtained, as shown in the following formula:

$$\frac{dr}{d\theta} = \frac{r^2 - r_d^2}{2rr_d} \tag{8}$$

We can obtain its solution as follows:

$$\begin{cases} r(\theta) = \dfrac{1 + k_r e^{-\theta}}{1 + k_r e^{-\theta}} r_d \\ k_r = \dfrac{r_0 - r_d}{r_0 + r_d} \end{cases} \tag{9}$$

where $r_0 = r(0)$ is the initial separation distance between the UAV and the target. Substituting this solution into the Eq. (6), we can obtain a function of time, as shown in the following formula:

$$\theta - \theta_0 = \frac{\mu_0}{r_d} t + 2k_r \left[\frac{e^{-\theta}}{1 - k_r e^{-\theta}} - \frac{e^{-\theta_0}}{1 - k_r e^{-\theta_0}}\right] \tag{10}$$

Here, θ_0 is the initial angular heading in polar coordinates. A certain type of UAV was taken as an example for the simulation. The initial values are set to $\mu_0 = 20m/s$, $r_d = 300m$, $x_0 = 800m$, and $y_0 = 800m$. Its trajectory is shown in Fig. 1:

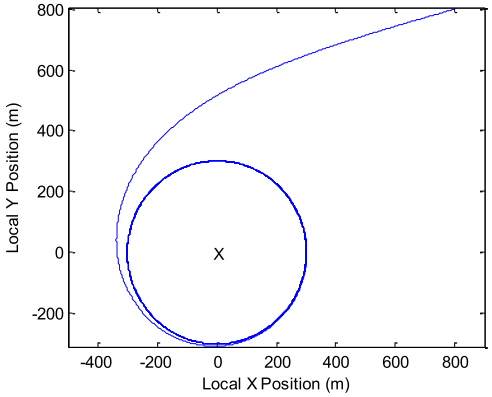

FIGURE 1. The trajectory of UAV in guidance vector filed.

The solutions to Eqs. (9) and (10) are complete analytical solutions; hence, the trajectory of the UAV is known. The angular heading along the vector field, denoted by ψ_d, is obtained by Eq. (11):

$$\psi_d = \arctan\left(\frac{\dot{y}}{\dot{x}}\right) = \arctan\left(\frac{y\left(r^2 - r_d^2\right) - x\left(2rr_d\right)}{x\left(r^2 - r_d^2\right) + y\left(2rr_d\right)}\right) \tag{11}$$

The derivative of Eq. (11) is given by

$$\dot{\psi}_d = \frac{4\mu_0 r_d^3}{\left(r^2 + r_d^2\right)^2} \tag{12}$$

To satisfy the constraints of the heading angular rate, we can obtain $\left|\dot{\psi}_d\right| < \omega_{\max}$, which is equivalent to $4\mu_0/r_d < \omega_{\max}$ using μ_0 and r_d.

According to Eq. (11), the UAV motion trajectory will converge to the desired circular orbit with the heading angle command, thus demonstrating that the initial heading is consistent with the direction of the guidance vector field. However, the initial heading is generally inconsistent with the guidance vector field. The following section will provide a way for the UAV to converge to the desired heading and prove it.

B. HEADING CONVERGENCE PROOF

A heading feedback method for obtaining rapid heading convergence was proposed by Summers *et al.* [1]; however, there was a lack of proof of the timescale separation between heading convergence and tracking radius convergence [15]. Other approaches use a dynamic sliding mode controller to ensure heading convergence in a finite time [16], [21], which

causes the actuator chatter under discontinuities and known external factors. This problem is solved by an approximation saturation function in theory; however, it is often neglected by scholars. In this section, a feedback convergence method is used to prove the convergence of the heading and solve the timescale separation problem. There are two theoretical and practical problems with UAVs tracking moving targets using this method. First, the feedback convergence proof is constrained by a set of initial headings; second, the kinematic constraints do not satisfy the requirements.

Aiming at the above first problem, a novel and simple method is proposed to ensure the convergence of the heading, which involves a loiter circle with an initial minimum radius. The UAV can converge exactly to the desired heading for any initial heading and is closely linked to the kinematic constraints. Further, the time and position convergence are fully analyzable, thus allowing the entire trajectory to be exactly known for any initial heading.

We introduce some additional notation for the guidance trajectory before the heading error analysis. Because $x = r\cos\theta$ and $y = r\sin\theta$, we define the angle ϕ, as shown in the Eq. (13):

$$\begin{cases} \cos\phi = \dfrac{r^2 - r_d^2}{r^2 + r_d^2} \\ \sin\phi = \dfrac{2rr_d}{r^2 + r_d^2} \end{cases} \tag{13}$$

and the dynamics Eq. (5) can be written as

$$\begin{aligned} \dot{x} &= -\frac{\mu_0}{r^2 + r_d^2}\left[(r^2 - r_d^2)\frac{x}{r} + (2rr_d)\frac{y}{r}\right] \\ &= -\mu_0\left[\sin\theta\cos\phi - \cos\theta\sin\phi\right] = -\mu_0\sin(\theta - \phi) \end{aligned} \tag{14}$$

According to Eqs. (11) and (14), we can obtain the following angle:

$$\psi_d = \theta - \phi + \pi \tag{15}$$

Suppose that the UAV's initial heading angle error ψ_d is defined by

$$\psi_e = \psi - \psi_d \tag{16}$$

Here, ψ is the real heading angle, and ψ_d is the desired heading angle. Suppose that the input command of the heading angle u_2 is defined by

$$\mu_2 = -k\psi_e + \dot{\psi}_d \tag{17}$$

Here, the feedback gain k is positive, and then, we obtain rapid convergence of the feedback error as $\psi_e(t) = \psi_{e0}e^{-kt}$. Here, $\psi_{e0} = \psi_e(0)$. Note that the parameter k controls the heading error convergence rate, and its selection directly affects the turn rate constraint, which requires a proper balance between the feedback and forward feedback. From Eqs. (1) and (16), the UAV dynamics are given by

$$\begin{cases} \dot{x} = \mu_1\cos(\psi_d)\cos(\psi_e) - \mu_1\sin(\psi_d)\sin(\psi_e) \\ \dot{y} = \mu_1\cos(\psi_d)\sin(\psi_e) + \mu_1\sin(\psi_d)\cos(\psi_e) \end{cases} \tag{18}$$

Here, when the heading error $\psi_e(t)$ converges to zero, the heading angle error matrix becomes the identity matrix, and the UAV formation along the guidance flight field in the desired trajectory. Based on Eqs. (11) and (18), we obtain the desired heading rate if there is a desired heading error, as shown in Eq. (19):

$$\begin{aligned} \dot{\psi}_d = \frac{4\mu_0 r_d^3}{(r^2 + r_d^2)} - \frac{2\mu_0}{r}\sin\left(\frac{\psi_e}{2}\right)\left(\cos(\phi)\cos\left(\phi - \frac{\psi_e}{2}\right)\right. \\ \left. - \sin(\phi)\sin\left(\phi - \frac{\psi_e}{2}\right)\right) \end{aligned} \tag{19}$$

Here, the desired heading rate consists of the ideal heading rate in Eq. (12). When ψ_e becomes zero, $\sin(\psi_e/2)$ is also zero; when the r in the denominator of Eq. (12) gradually becomes small, the desired heading angular rate may produce a larger command.

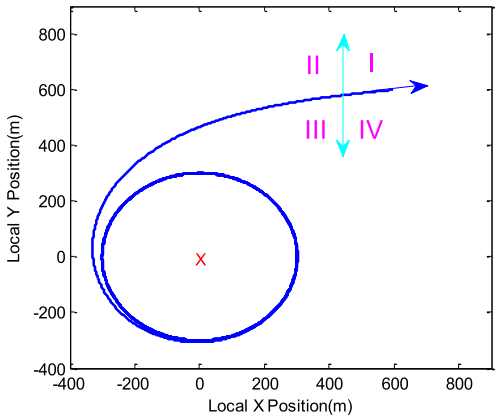

FIGURE 2. The quadrant of the heading error.

The boundedness and convergence of the heading feedback method depends on the quadrant of the initial heading error [1]. An example is illustrated in Fig. 2. Its initial condition is as follows: $\mu_0 = 20m/s$, $r_d = 300m$, $x_0 = 600m$ and $y_0 = 600m$. The desired heading angle is tangent to this trajectory; the actual initial heading will be inconsistent with the guidance vector field, but the initial heading is located in the direction of one of the four quadrants.

III. TRACKING CONTROLLER DESIGN

Based on the second section on stationary targets and conditions with wind, the proposed the Lyapunov guidance vector field method is extended to address unknown wind conditions and moving targets. Here, we use variable airspeed control and the wind's adaptive estimates to maintain a circular orbit model. In general, the moving target has the same characteristics, which restricts us to considering the moving target with a constant forward velocity. However, this method can be applied to multi-UAVs tracking a moving target at a constant velocity. We also discuss the limitations of the theory and practice and design a controller with the given kinematic constraints.

A. VARIABLE AIRSPEED CONTROLLER DESIGN

The UAV's kinematic equation is given by Eq. (1). It represents the mathematical model relative to the moving target. The model for including wind is as follows:

$$\begin{cases} \dot{x} = \mu_1 \cos\psi + W_x - V_{xT} \\ \dot{y} = \mu_1 \sin\psi + W_y - V_{yT} \\ \dot{\psi} = \mu_2 \end{cases} \tag{20}$$

where $[W_x, W_y]^T$ represents the component of a constant wind velocity in along two axes, $[W_{xT}, W_{yT}]^T$ represents the component of the constant inertial target velocity along the two axes. The wind velocity and target velocity both affect the kinematics of the model, and we combine the two effects into one variable, as shown in Eq. (21):

$$\begin{cases} T_x = V_{xT} - W_x \\ T_y = V_{yT} - W_y \end{cases} \tag{21}$$

We treat T_x and T_y as unknown constants, and we suppose the availability of the upper bound; hence, T^* satisfies the following formula:

$$\max\left(T_x, T_y\right) \le T^* \tag{22}$$

It encompasses the worst case of the wind and motion target velocities in the coupling effect. Consider the following controller design:

$$\begin{cases} \mu_1 \cos\psi = -\mu_0 \cos\left(\theta - \phi\right) + \hat{T}_x - \upsilon_s \sin\theta \\ \mu_1 \sin\psi = -\mu_0 \sin\left(\theta - \phi\right) + \hat{T}_y + \upsilon_s \cos\theta \end{cases} \tag{23}$$

Here, $\hat{T}_x$ and $\hat{T}_y$ present adaptive estimates in the case of unknown wind and moving targets, υ_s represents a specific signal, and all other symbols have the same meaning as before. We define a heading as follows:

$$\tan\psi = \frac{-\mu_0 \sin\left(\theta - \phi\right) + \hat{T}_y + \upsilon_s \cos\theta}{-\mu_0 \cos\left(\theta - \phi\right) + \hat{T}_x - \upsilon_s \sin\theta} \tag{24}$$

The airspeed input is as follows:

$$\mu_1^2 = \left[-\mu_0 \sin\left(\theta - \phi\right) + \hat{T}_y + \upsilon_s \cos\theta\right]^2 + \left[-\mu_0 \cos\left(\theta - \phi\right) + \hat{T}_x - \upsilon_s \sin\theta\right]^2 \tag{25}$$

The heading angle is given by Eq. (24); it is different from the obtained heading rate input. Combining Eqs. (24) and (20), we obtain Eq. (26), as shown in the following formula:

$$\begin{cases} \dot{r} = -\mu_0 \dfrac{r^2 - r_d^2}{r^2 + r_d^2} + \tilde{T}_x \cos\theta + \tilde{T}_y \sin\theta \\ r\dot{\theta} = -\mu_0 \dfrac{2rr_d}{r^2 + r_d^2} - \tilde{T}_x \sin\theta + \tilde{T}_y \cos\theta + \upsilon_s \end{cases} \tag{26}$$

where $\tilde{T}_x = \hat{T}_x - T_x$ and $\tilde{T}_y = \hat{T}_y - T_y$ are adaptive estimation errors. We use the same Lyapunov guidance vector field to define relative motion in the ideal case, as shown in Eq. (27):

$$\begin{cases} \dot{r}_p = -\mu_0 \dfrac{r_p^2 - r_d^2}{r_p^2 + r_d^2} \\ r_p\dot{\theta}_p = -\mu_0 \dfrac{2r_p r_d}{r_p^2 + r_d^2} \end{cases} \tag{27}$$

where r_p represents the radius of the moving trajectory in the Lyapunov guidance vector.

The defined error signal is given by

$$\begin{cases} e_r = r - r_p \\ e_\theta = \theta - \theta_p \end{cases} \tag{28}$$

and from Eq. (26) and the derivative of Eq. (28), the response error dynamics are given by

$$\begin{cases} \dot{e}_r = -\mu_0 \dfrac{2r_d^2\left(r^2 - r_p^2\right)e_r}{\left(r^2 + r_d^2\right)\left(r^2 + r_p^2\right)} + \tilde{T}_x \cos\theta + \tilde{T}_y \sin\theta \\ \dot{e}_\theta = -\mu_0 \dfrac{2r_d^2\left(r^2 + r_p^2\right)e_r}{\left(r^2 + r_d^2\right)\left(r^2 + r_p^2\right)} \\ \qquad + \dfrac{1}{r}\left(-\tilde{T}_x \sin\theta + \tilde{T}_y \cos\theta + \upsilon_s\right) \end{cases} \tag{29}$$

The actual trajectory and guidance filed trajectory have the same curve, which shows that $r_p(0) = r(0)$ and $\theta_p(0) = \theta(0)$. Therefore, when the heading angle converges to the angle corresponding to the Lyapunov guidance vector field, the error signal is zero at the initial time.

If the UAV can obtain desired heading angle before the adaptive process is initialized, the UAV can accurately track the moving target with the desired trajectory. Hence, it is important to obtain the desired heading angle before the adaptive process is initialized. Moreover, the built model offers some flexibility and facilitates subsequent analysis, while the adaptive estimates $\hat{T}_x$ and $\hat{T}_y$ are also initialized. The desired heading angle does not have to be fully known, but we can be close to the exact heading angle using pattern recognition. When the target does not enter the initial loiter circle, we have obtained the exact heading angle.

For some initial conditions and target trajectory, the heading angle of the UAV does not convergence to the desired heading angle within a loiter circle. Suppose that the desired heading angle of the moving target is obtained before entering the initial set circle, which will be achieved. However, the target will eventually exit the circular trajectory because the target moves at a constant velocity. Hence, the desired heading angle will be achieved, but it may need additional oscillations to converge to the desired circle. For simplicity, we believe that there is sufficient initial separation time so that the desired heading angle can achieve the purpose of separation within the scope of the initial loiter circle orbit. Thus, the required time for the target to move in a circular orbit will be applied to the variable velocity control scheme design.

B. STABILITY ANALYSIS

Before analyzing the stability, a parametric projection relationship was introduced to ensure that the moving target estimates evolve within the scope of the given T^*.

We define new variables, as shown in Eq. (30):

$$\begin{cases} \hat{T}_x = T^* \tanh \hat{\phi}_x \\ \hat{T}_y = T^* \tanh \hat{\phi}_y \end{cases} \tag{30}$$

where $\hat{\phi}_x$ and $\hat{\phi}_y$ represent the unconstrained estimates, and the actual parameter values of the response are as follows:

$$\begin{cases} T_x = T^* \tanh \phi_x^* \\ T_y = T^* \tanh \phi_y^* \end{cases} \tag{31}$$

Consider the Lyapunov function, as shown in Eq. (32):

$$V = \frac{1}{2} e_r^2 + (\mu/2)\, e_\theta^2 + \left(T^*/\gamma\right)\left(\log\cosh \hat{\phi}_x - \hat{\phi}_x \tanh \phi_x^*\right) + \left(T^*/\gamma\right)\left(\log\cosh \hat{\phi}_y - \hat{\phi}_y \tanh \phi_y^*\right) + c^* \tag{32}$$

where c^* represents a to-be-determined constant value. For any $\mu > 0$ and $\gamma > 0$, the function $V(t)$ is positive definite. According to the defined trajectory in Eq. (29), we calculate the derivative of $V(t)$, and we define the adaptive update algorithm, as shown in the following formula:

$$\begin{cases} \dot{\hat{\theta}}_x = -\gamma \left[e_r \cos\theta - \mu \dfrac{e_\theta \sin\theta}{r} \right] \\ \dot{\hat{\theta}}_y = -\gamma \left[e_r \sin\theta + \mu \dfrac{e_\theta \cos\theta}{r} \right] \\ \upsilon_s = -\dfrac{k_\theta \mu_0}{\gamma} \tanh e_\theta + \beta \end{cases} \tag{33}$$

For the signal β and the positive constant k_θ, we obtain

$$\dot{V} = -\mu_0 \mu \mu_0 \frac{2 r_d^2 \left(r^2 - r_p^2\right) e_r^2}{\left(r^2 + r_d^2\right)\left(r^2 + r_p^2\right)} - \frac{k_\theta}{r} e_\theta \tanh e_\theta - \mu \mu_0 \frac{2 r_d \left(r + r_p\right) e_r e_\theta}{\left(r^2 + r_d^2\right)\left(r^2 + r_p^2\right)} + \frac{\mu \beta e_\theta}{r} \tag{34}$$

where the parameter γ represents the rate of an adaptive learning, which controls how quickly to adapt to Eq. (33). To eliminate the uncertainty of the signal in Eq. (35), we define β as follows in Eq. (35):

$$\beta = \frac{2 \mu_0 r_d \left(r + r_p\right) r e_r}{\left(r^2 + r_d^2\right)\left(r^2 + r_p^2\right)} \tag{35}$$

We also obtain

$$\dot{V} = -\mu_0 \frac{2 r_d^2 \left(r^2 - r_d^2\right) e_r^2}{\left(r^2 + r_d^2\right)\left(r^2 + r_p^2\right)} - \frac{k_\theta \mu_0}{\gamma r} e_\theta \tanh e_\theta \le 0 \tag{36}$$

From Eqs. (26) and (30), we easily find that the Lyapunov function is less than zero if $\gamma > 0$. The constant c^* is still to be determined in Eq. (32). Since the initial values of the errors e_r and e_θ are zero, it is assumed that the initial values of the adaptive estimation $\hat{\phi}_x$ and $\hat{\phi}_y$ are also zero, and $\hat{\phi}_x = \phi_x^*$ and $\hat{\phi}_y = \phi_y^*$, where the third and fourth orders of the function have a minimum value. To prove the positive definiteness of the Lyapunov function, we define c^*, as shown in the following formula:

$$c^* = \left(T^*/\gamma\right) \left[\begin{array}{l} \left|\log\cosh \phi_x^* - \phi_x^* \tanh \phi_x^*\right| \\ \quad + \left|\log\cosh \phi_y^* - \phi_y^* \tanh \phi_y^*\right| \end{array} \right] \tag{37}$$

where c^* is inversely proportional to γ, and $1/2 e_r^2 \le V(t) \le V(0) = c^*$; here, $|e_r(t)| \le \sqrt{2c^*}$.

According to the above formulas, we establish the upper bound of c^*, as shown in the following formula:

$$c^* \le \frac{2 \log 2 T^*}{\gamma} \tag{38}$$

Therefore, the maximum radius error of the trajectory of the moving target is reduced by increasing the learning rate parameter γ.

C. KINEMATIC CONSTRAINTS

There are theoretical and practical limitations to the controller given the kinematic constraint Eqs. (2) and (3). For example, when the velocities of the wind and moving target are too large, the UAV will not be able to maintain flight in a circular orbit around the target. Moreover, even if the UAV is kept in a circular orbit, strong airspeed variations are required, but this controller design is infeasible from the perspective of fuel efficiency. For this case, we check the UAV command to establish a positive parameter α, as shown in the following formula:

$$T^* = \alpha \mu_0 \tag{39}$$

For the maximum target velocity T^*, we consider the airspeed constraint Eq. (2) and establish Eq. (41), as shown in the following equation:

$$\mu_1^2 = \mu_0^2 + \upsilon_s^2 + \hat{T}_x^2 + \hat{T}_y^2 + 2\mu_0 \upsilon_s \sin\phi + \hat{T}_y \sin(\theta - \phi) + 2\upsilon_s \left(\hat{T}_y \cos\theta - \hat{T}_x \sin\theta\right) - 2\upsilon_0 \left(\hat{T}_x \cos(\theta - \phi)\right) \tag{40}$$

Combining Eqs. (22) and (39), we obtain the following upper bound:

$$\mu_1^2 \le \left[|\upsilon_s| + \mu_0 (1 + 2\alpha)\right]^2 \tag{41}$$

To satisfy the airspeed constraint, we require that $\mu_1^2 \le \mu_{\max}^2$. We can obtain Eq. (43) as follows:

$$\alpha < \frac{1}{2} \left[\frac{\upsilon_{\max}}{\mu_0} - 1 \right] \tag{42}$$

Further, from Eq. (40), we establish the lower bound on the commanded airspeed, as shown in Eq. (43):

$$\mu_1^2 \ge |\upsilon_s|^2 - 2\mu_0 (1 + 2\alpha) |\upsilon_s| + (1 - 4\alpha) \mu_0^2 \tag{43}$$

To satisfy the airspeed constraint, $\mu_1^2 \geq \mu_{\min}^2$ is required; thus, we obtain

$$|\upsilon_s|^2 - 2\mu_0 (1+2\alpha) |\upsilon_s| + (1-4\alpha)\mu_0^2 - \upsilon_{\min}^2 \geq 0 \quad (44)$$

In addition, we can obtain the two roots r^+ and r^- of Eq. (46), as shown in Eq. (47):

$$|\upsilon_s|^2 - 2\mu_0 (1+2\alpha) |\upsilon_s| + (1-4\alpha)\mu_0^2 - \upsilon_{\min}^2 = 0 \quad (45)$$

$$\begin{cases} r^+ = \mu_0 (1+2\alpha) + \sqrt{4\alpha^2\mu_0^2 + 8\alpha\mu_0^2 + \upsilon_{\min}^2} \\ r^+ = \mu_0 (1+2\alpha) - \sqrt{4\alpha^2\mu_0^2 + 8\alpha\mu_0^2 + \upsilon_{\min}^2} \end{cases} \quad (46)$$

We easily obtain that $r^+ > r^-$. Thus, Eq. (45) can be simplified as Eq. (48):

$$\left(|\upsilon_s| - r^+\right)\left(|\upsilon_s| - r^-\right) \geq 0 \quad (47)$$

To satisfy the above conditions, we require that $|\upsilon_s| \geq r^+$ or $|\upsilon_s| \leq r^-$. Because we are only concerned with the upper bound $|\upsilon_s|$, we adopt $|\upsilon_s| \leq r^-$, which gives

$$|\upsilon_s| \leq \mu_0 (1+2\alpha) - \sqrt{4\alpha^2\mu_0^2 + 8\alpha\mu_0^2 + \upsilon_{\min}^2} \quad (48)$$

For the above formula to be meaningful, we need the right-hand side of the inequality to be positive, which will generate a separate upper bound for α, as shown in the following formula:

$$\alpha < \frac{1}{4}\left[1 - \frac{\upsilon_{\min}^2}{\mu_0^2}\right] \quad (49)$$

Combine Eqs. (43) and (49), we obtain

$$\alpha < \min\left[\frac{1}{2}\left(\frac{\upsilon_{\max}}{\mu_0} - 1\right), \frac{1}{4}\left(1 - \frac{\upsilon_{\min}^2}{\mu_0^2}\right)\right] = \alpha_{\max} \quad (50)$$

To satisfy the airspeed constraint in Eq. (2), we need $0 \leq \alpha \leq \alpha_{\max}$ to satisfy $T^* = \alpha\mu_0$. From Eq. (48), there must be a limit between the allowable airspeed variable and the allowable wind and target speeds.

Within the range of larger allowable airspeeds, a faster moving target or stronger wind can be accommodated in this environment.

The lower bound is established for the learning rate γ to satisfy the airspeed constraint of Eq. (2). Because $r = e_r + e_p$, we obtain $|r| \leq |e_r| + |r_p|$. In addition, for any t and $r_0 \geq |r_p| \geq r_d$, we can obtain $|e_r| \leq \sqrt{2c^*}$. However, we can obtain the upper bound of β in Eq. (34), as shown in Eq. (51):

$$|\beta| \leq \frac{2\mu_0\sqrt{2c^*}\left(\sqrt{2c^*} + r_0\right)\left(\sqrt{2c^*} + 2r_0\right)}{r_d^3} \quad (51)$$

Combining Eqs. (34), (47) and (51), we establish Eq. (52), as shown in the following formula:

$$\frac{k_\theta}{\gamma} + \frac{2\sqrt{2c^*}\left(\sqrt{2c^*} + r_0\right)\left(\sqrt{2c^*} + 2r_0\right)}{r_d^3} \leq \min\left[\frac{\frac{\upsilon_{\max}}{\mu_0} - (1+2\alpha)}{-\sqrt{4\alpha^2 + 8\alpha + \frac{\upsilon_{\min}^2}{\mu_0^2}}}\right] \quad (52)$$

Solving Eq. (52) yields a lower bound of γ so that we can satisfy the requirement from the airspeed constraint. However, we cannot arbitrarily choose the depth learning rate γ because there is a potentially isolated heading angular rate constraint in Eq. (52). We obtain the heading angular rate from the derivative of Eq. (25). The adaptive estimates given in Eq. (34) are proportional to Eq. (31) and inversely proportional to the learning rate γ. Therefore, we choose a suitable learning rate γ to satisfy the heading rate constraint.

To satisfy the airspeed constraint, it is important to choose the upper and lower boundaries in this section. In addition, the selection process for the different boundaries is conservative, which is apparent in the process of the simulation so that we constantly update the dates. In practice, the design criteria of the different loiter circles will ultimately depend on the performed missions of the UAV. The proposed controller allows adjustable parameters such that the process of tracking can address the uncertainties while also satisfying the kinematic constraints.

IV. FORMATION INFORMATION ARCHITECTURE

In this section, we establish the structure of the UAV formation using graph theory [12], [22]–[26], and we further study the information architecture. We establish the connection between the controller design and the cooperative tracking problem, and we also establish an information architecture with distributed control laws.

The fundamental task of the UAV formation control is to maintain the prescribed formation shape with an optimal formation distribution. This section mainly concerns the information architecture of the UAV formation in satisfying the formation geometric shape.

In the theory of combinatorial methods [17], [27], the notation of the rigidity graph is used to describe the information construct of the UAV formation for satisfying the formation geometric shape. In general, a formation is rigid if the UAV formation moves as a whole or rotates about a fixed axis with the relative distance preserved between them. We desire the UAV formation to be maintained.

There are two methods for controlling the relative distance between any two UAVs. First, the relative distance between any two designated UAVs remains constant, and second, the relative distance between any UAV and the remaining UAVs in formation remains constant. This method generates two types of information architectures: symmetric and

asymmetric architectures. The symmetric architectures are modeled using an undirected graph, whereas the asymmetric architectures of the UAV formation are modeled using a directional graph.

A. MODELING A MULTI-UAV SYSTEM

Suppose that there are N(N = 3) UAVs with the same motion characteristics, including N−1 followers and a leader, thereby constituting a UAV formation system. With regard to a multi-UAV system with bidirectional network links between the UAVs, any two UAVs of the formation system will exchange information with each other. This network can be mathematically described using graph theory [17]. Thus, the UAV formation system has a network topology, as shown in Fig. 3:

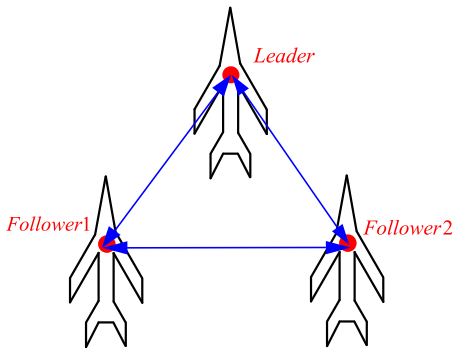

FIGURE 3. The UAV formation system of the network topology.

For a graph $G = (V, E)$, V is a set of vertices, $|V|$ is the order of graph G, E is a set of edges, and $|E|$ is the number of sides of graph G [28]. In this paper, we use a graph $G = (V, E)$ to establish the information interaction relationship between n UAVs, where $V = \{v_1, v_2, v_3, \cdots, v_N\}$ is a set of vertices and $E \in V \times V$ is a set of edges. The edge (v_i, v_j) in E represents that there is a network path from UAV i to the UAV j, that is, UAV j can obtain and use information from UAV i. A directed tree is a graph G, including all nodes. Every node acts as a parent node except for itself, called a root node. In a directed graph, the root node cannot be directly connected to the parent node but can be directly connected with other nodes. However, in an undirected graph, the edge (v_i, v_j) indicates that UAV i and UAV j can exchange information with each other; in other words, (v_i, v_j) and (v_j, v_i) are the same. Let $A \in R^{N\times N}$, $D \in R^{N\times N}$ and $L \in R^{N\times N}$ be an adjacency matrix, a degree matrix, and a graph Laplacian matrix, respectively. Here, A represents the relationship between nodes in graph theory, and based on graph theory, the neighbor matrix $A = [a_{ij}]$ is given by

$$a_{ij} = \begin{cases} 1, & (v_i, v_j) \in A \\ 0, & (v_i, v_j) \notin A \end{cases} \tag{53}$$

From the above equation, if UAV i is directly obtaining information from UAV j, $a_{ij} = 1$; otherwise, $a_{ij} = 0$. The degree matrix D represents an in-degree matrix given by

$$D = diag(\deg(v_1), \deg(v_2), \cdots, \deg(v_N)) \tag{54}$$

where $\deg(v_i)$ is the communication sum number of node v_i with other nodes. The graph Laplacian matrix L is defined as [29]

$$L = [l_{ij}] \in R^{n\times n}, \quad l_{ij} = \sum_{i\neq j} a_{ij}, \quad l_{ij} = -a_{ij}\ (i \neq j) \tag{55}$$

From the above equation, the matrix L has the following two properties:

1) $l_{ij} < 0, i \neq j, \sum_{j=1}^{n} l_{ij} = 0, i = 1, 2, \cdots n.$

Definition 1_n denotes an N-dimensional column vector of all elements that are 1, and 0_n denotes an N-dimensional column vector of all elements that are 0. According to the definition of the Laplace matrix, the following equation holds: $L1_n = 0_n$ [30].

2) $L = D - A$. If a graph G has a directed spanning tree, the matrix L has a single eigenvalue at zero, and all nonzero eigenvalues of the graph Laplacian have positive real parts.

B. MULTI-UAV TARGET TRACKING

Our objective is divided into static and motion; this section concerns a stationary target. We can achieve the desired angular spacing by designing the distributed control laws of the UAV formation. We propose two methods of information architectures based on the previous section. The first method is an asymmetric persistent leader-follower method. The second method is the non-minimally persistent leader-follower method. Each UAV uses a variable airspeed controller to obtain the desired spacing. We obtain the desired angular spacing by adjusting the allowable range of airspeed variations without affecting our convergence properties with minimal losses. Here, there is trade-off whereby a larger allowable airspeed means faster convergence and a smaller allowable airspeed means slower convergence. Many scholars have studied the larger symmetry structures; therefore, there is no need to repeat the arguments. This section main studies the non-minimally persistent symmetric information architecture.

1) Control law design and stability analysis

In this paper, the control objects consist of the formation of three UAVs and a target. The dynamics of the ith UAV are modeled in polar coordinates, as shown in the following formula:

$$\begin{cases} \dot{r}_i = -\mu_{1i}\dfrac{r_i^2 - r_d^2}{r_i^2 + r_d^2} \\ r_i\dot{\theta}_i = \mu_{1i}\dfrac{2r_i r_d}{r_i^2 + r_d^2}, \quad i = 1, \cdots, n \end{cases} \tag{56}$$

Suppose that the n th UAV has a constant airspeed, as shown in Eq. (57):

$$\mu_{1n} = \mu_0 \tag{57}$$

In addition, the airspeed inputs of the remaining $n-1$ UAVs are given by

$$\mu_{1i} = \mu_0 + \Delta V_{\max} \tanh\left(\theta_{i+1} - \theta - \theta_d\right) \frac{r_i^2 + r_d^2}{r_{i+1}^2 + r_i^2} \tag{58}$$

where $\Delta V_{\max} > 0$ is a design parameter used to satisfy the constraint of Eq. (58). θ_d is the desired angular spacing between any two UAVs. To satisfy the airspeed constraint, we require that $\mu_0 - \Delta V_{\max} > \upsilon_{\min} > 0$, and the second part of the right-hand side of the equation adjusts to compensate the error between them. When the desired spatial position is achieved, the second part becomes zero, and the airspeed also becomes a constant μ_0. For any positive value $\Delta V_{\max}$, we can achieve the desired spatial position; therefore, the allowable airspeed variation range can ensure the maximum utilization of fuel. When we choose a smaller value of the loiter circle at $\Delta V_{\max}$, the convergence speed of the desired angular spacing may be lower.

We define the angular spacing errors as $\delta\theta_i = \theta_{i+1} - \theta_i - \theta_d$, and then, we differentiate and combine Eq. (57). We thereby obtain the angular spacing error dynamics:

$$\begin{cases} \delta\dot{\theta}_{n-1} = \dfrac{2\mu_0 r_d \left(r_{n-1}^2 - r_n^2\right)}{\left(r_n^2 + r_d^2\right)\left(r_{n-1}^2 + r_d^2\right)} - \dfrac{2r_d \Delta V_{\max}}{\left(r_n^2 + r_{n-1}^2\right)} \\ \qquad \times \tanh\left(\delta\theta_{n-1}\right) - \dfrac{2r_d \Delta V_{\max}}{\left(r_{i+1}^2 + r_i^2\right)}, \quad i = n-1 \\ \delta\dot{\theta}_i = \dfrac{2\mu_0 r_d \left(r_i^2 - r_{i+1}^2\right)}{\left(r_{i+1}^2 + r_d^2\right)\left(r_i^2 + r_d^2\right)} - \dfrac{2r_d \Delta V_{\max}}{\left(r_{i+2}^2 + r_{i+1}^2\right)} \\ \qquad \times \tanh\left(\delta\theta_{i+1}\right) - \dfrac{2r_d \Delta V_{\max}}{\left(r_{i+1}^2 + r_i^2\right)} \tan(\delta\theta_i), \\ \qquad\qquad i = 1, \cdots, n-2 \end{cases} \tag{59}$$

Now, consider the Lyapunov function, as shown in the follow equation:

$$V = \sum_{i=1}^{n-1} \log\cosh \delta\theta_i + \frac{1}{2} \sum_{i=1}^{n} \lambda_i \gamma_i^2 \tag{60}$$

Choosing a suitable parameter λ, the trajectories are defined by Eqs. (57) and (60). Then, calculating the derivative of the function V, we obtain

$$\begin{aligned} \dot{V} = & \sum_{i=1}^{n-1} \left[\frac{2\mu_0 r_d}{\left(r_{i+1}^2 + r_d^2\right)\left(r_i^2 + r_d^2\right)} \tanh\left(\delta\theta_i\right) \right. \\ & \left. - \frac{2r_d \Delta V_{\max}}{\left(r_{i+1}^2 + r_i^2\right)} \tanh^2\left(\delta\theta_i\right) - \lambda_i r_i \mu_{1i} \frac{r_i^2 - r_d^2}{r_i^2 + r_d^2} \right] \\ & + \sum_{i=1}^{n-2} \left[\frac{2r_d \Delta V_{\max}}{\left(r_{i+2}^2 + r_{i+1}^2\right)} \tanh\left(\delta\theta_{i+1}\right) \tanh\left(\delta\theta_i\right) \right] \\ & - \lambda_n r_n \mu_0 \frac{r_n^2 - r_d^2}{r_n^2 + r_d^2} \end{aligned} \tag{61}$$

Combining the $r_d \le r_i(t) \le r_{i0}$ of Eq. (56) and the $\mu_{12} \ge \mu_0 - \Delta V_{\max}$ of Eq. (59), we obtain the upper bound of the derivative $\dot{V}$ as

$$\begin{aligned} \dot{V} \le & \sum_{i=1}^{n-1} \left[-\frac{\Delta V_{\max}}{\bar{r}_0^2} \tanh^2 \delta\theta_i + \frac{\mu_0 \left(r_i^2 - r_d^2\right)}{r_d \left(r_i^2 + r_d^2\right)} \right. \\ & \left. + \frac{\mu_0 \left(r_{i+1}^2 - r_d^2\right)}{r_d \left(r_{i+1}^2 + r_d^2\right)} - \lambda_i r_d (\mu_0 - \Delta V_{\max}) \frac{\left(r_i^2 - r_d^2\right)}{\left(r_i^2 + r_d^2\right)} \right] \\ & + \sum_{i=1}^{n-2} \left[\frac{\Delta V_{\max}}{r_d} \tanh\left(\delta\theta_{i+1}\right) \tanh(\delta\theta_i) \right] \\ & - \lambda_n r_n \mu_0 \frac{r_n^2 - r_d^2}{r_n^2 + r_d^2} \end{aligned} \tag{62}$$

Eq. (58) can be simplified as

$$\begin{aligned} \dot{V} \le & -\tanh \delta\theta^T C \tanh \delta\theta \\ & - \sum_{i=1}^{n-1} \left[\left[\lambda_n r_d \left(\mu_0 - \Delta V_{\max}\right) - \frac{2\mu_0}{r_d} \right] \frac{\left(r_n^2 - r_d^2\right)}{\left(r_n^2 + r_d^2\right)} \right] \end{aligned} \tag{63}$$

where $\tanh \delta\theta = [\tanh(\delta\theta_1), \cdots, \tanh(\delta\theta_{n-1})]$, and the positive-definite form of the matrix C is given by (64), as shown at the bottom of this page.

We choose:

$$\begin{cases} \lambda_i > \left(\mu_0 / r_d^2\right)\left(\mu_0 - \Delta V_{\max}\right), \quad i = 1, \cdots, n-1 \\ \lambda_n > \left(1 / r_d^2\right) \end{cases} \tag{65}$$

We then obtain $\dot{V} \le 0$; this implies

$$\lim_{t \to \infty} r_i(t) = r_d, \forall i \tag{66}$$

$$C = \begin{bmatrix} \dfrac{\Delta V_{\max} r_d}{\bar{r}_0^2} & -\dfrac{\Delta V_{\max}}{r_d} & 0 & \cdots & 0 \\ 0 & \dfrac{\Delta V_{\max} r_d}{\bar{r}_0^2} & -\dfrac{\Delta V_{\max}}{r_d} & \cdots & 0 \\ 0 & \cdots & \ddots & \cdots & 0 \\ 0 & \cdots & 0 & \dfrac{\Delta V_{\max} r_d}{\bar{r}_0^2} & -\dfrac{\Delta V_{\max}}{r_d} \\ 0 & 0 & \cdots & 0 & \dfrac{\Delta V_{\max} r_d}{\bar{r}_0^2} \end{bmatrix} \tag{64}$$

We also obtain the radius of the loiter circle and satisfy $\lim_{t\to\infty} \delta\theta_i(t) = 0, \forall i$; thus, we can achieve the control of the angular spacing.

2) Non-minimum persistent information architecture

For the symmetric information architecture for UAV formation, we design a control law based on the asymmetric minimum persistent information architecture. We adjust the airspeed so that a single UAV moves toward the midpoint of its two adjacent UAVs, thereby constituting the three-UAV formation. Although this structure does not contain the minimum possible number of information links, it can achieve the control of the angular spacing whereby we do not need to know the number of UAVs. This section mainly studied the control law design and stability analysis. The dynamics are given by Eq. (56), and the airspeed command of the ith UAV is given by

$$\mu_{1i} = \mu_0 - \Delta V_{\max} \tanh \delta_i \frac{\gamma_i^2 + r_d}{r_{i-1}^2 + r_i^2 + r_{i+1}^2} \tag{67}$$

where $\Delta V_{\max} > 0$ represents a design parameter and the inputs satisfy the airspeed constraint. For any given positive value $\Delta V_{\max}$, we can achieve the desired angular spacing. Thus, the allowable variation can be adjusted to improve the fuel efficiency of the UAV formation. The angular spacing error of the ith UAV is defined by

$$\delta\theta_i = \theta_i - \frac{1}{2}(\theta_{i-1} + \theta_{i+1}) \tag{68}$$

There are n modulo cycles around the loiter circle, as shown in the following formula:

$$\theta_0 = \theta_n - 2\pi, \theta_{n+1} = \theta_1 + 2\pi \tag{69}$$

The derivative of Eq. (68) is given by

$$\begin{aligned}
&\dot{\delta\theta_i} \\
&= -\Delta V_{\max} \frac{r_d}{R_i^2} \left(2\tanh(\delta\theta_i) + \tanh(\delta\theta_{i+1}) + \tanh(\delta\theta_{i-1})\right) \\
&\quad + \frac{r_d\mu_0\left(r_{i+1}^2 - r_d^2\right)}{\left(r_i^2 + r_d^2\right)\left(r_{i+1}^2 + r_d^2\right)} + \frac{r_d\mu_0\left(r_{i-1}^2 - r_d^2\right)}{\left(r_i^2 + r_d^2\right)\left(r_{i-1}^2 + r_d^2\right)} \\
&\quad - \frac{r_d\mu_0\left(r_i^2 - r_d^2\right)}{\left(r_i^2 + r_d^2\right)\left(r_{i+1}^2 + r_d^2\right)} - \frac{r_d\mu_0\left(r_i^2 - r_d^2\right)}{\left(r_i^2 + r_d^2\right)\left(r_{i-1}^2 + r_d^2\right)}
\end{aligned} \tag{70}$$

Here, $R_i^2 = \sum_{j-1}^{j+1} r_i^2$. Consider the Lyapunov function

$$V = \sum_{i=1}^{n} \left[\log\cosh\left(\delta\dot{\theta}_i\right) + \frac{\lambda}{2} r_i^2\right] \tag{71}$$

where $\lambda > 0$. We can obtain the upper bound of the derivative of V, and we combine Eqs. (56) and (69) and $\mu_{12} \geq \mu_0 - \Delta V_{\max}$, $r_d \leq r_i(t) \leq r_{i0}$, as shown in the following formula:

$$\begin{aligned}
\dot{V} \leq -\Delta V_{\max} \frac{r_d}{R_i^2} \Big[&(|\tanh\delta\theta_1| - |\tanh\delta\theta_2|)^2 \\
&+ (|\tanh\delta\theta_2| - |\tanh\delta\theta_3|)^2 \\
&+ \cdots + (|\tanh\delta\theta_{n-1}| - |\tanh\delta\theta_n|)^2 \\
&+ (|\tanh\delta\theta_n| - |\tanh\delta\theta_1|)^2\Big] \\
+ \sum_{i=1}^{n} \left[\frac{2\mu_0}{r_d} - \lambda r_d(\mu_0 - \Delta V_{\max})\right] &\frac{r_i^2 - r_d^2}{r_i^2 + r_d^2}
\end{aligned} \tag{72}$$

We choose

$$\lambda > \frac{2\mu_0}{r_d^2(\mu_0 - \Delta V_{\max})} \tag{73}$$

When $\dot{V} \leq 0$,

$$\lim_{t\to\infty} |\tanh\delta\theta_i| = \bar{T} \quad \forall i \tag{74}$$

where $\bar{\theta}$ and $\bar{T}$ are finite constants. For any i, we obtain $\delta\theta_i = \bar{\theta}$ when $t \to \infty$.

Now, we define the angular error, as shown in the following formula:

$$\begin{cases}
e_{12} = \theta_1 - \theta_2 \\
e_{23} = \theta_2 - \theta_3 \\
\vdots \\
e_{n-1,n} = \theta_{n-1} - \theta_n \\
e_{n1} = \theta_n - \theta_1
\end{cases} \tag{75}$$

and when $t \to \infty$, we can obtain the relationship of between the angular spacing and the angular error from Eqs. (68) and (75) as follows:

$$\begin{aligned}
\begin{bmatrix} \delta\theta_1 \\ \delta\theta_2 \\ \delta\theta_3 \\ \vdots \\ \delta\theta_{n-1} \\ \delta\theta_n \end{bmatrix} &= \begin{bmatrix} \bar{\theta} \\ \bar{\theta} \\ \bar{\theta} \\ \vdots \\ \bar{\theta} \\ \bar{\theta} \end{bmatrix} \\
&= \begin{bmatrix}
\frac{1}{2} & 0 & 0 & \cdots & 0 & -\frac{1}{2} \\
-\frac{1}{2} & \frac{1}{2} & 0 & 0 & \cdots & 0 \\
0 & -\frac{1}{2} & \frac{1}{2} & 0 & \cdots & 0 \\
\vdots & \cdots & \ddots & \ddots & 0 & 0 \\
0 & \cdots & 0 & -\frac{1}{2} & \frac{1}{2} & 0 \\
0 & 0 & \cdots & 0 & -\frac{1}{2} & \frac{1}{2}
\end{bmatrix} \\
&\quad \times \begin{bmatrix} e_{12} \\ e_{23} \\ e_{34} \\ \vdots \\ e_{n-1,n} \\ e_{n1} \end{bmatrix} + \begin{bmatrix} \pi \\ 0 \\ 0 \\ \vdots \\ 0 \\ -\pi \end{bmatrix}
\end{aligned} \tag{76}$$

Further, the sum of all the angular differences is zero as follows:

$$e_{12} + e_{23} + e_{34} + \cdots + e_{n-1,n} + e_{n1} = 0 \tag{77}$$

From Eq. (77), we can see that there are $n + 1$ equations to be solved. Solving the $n + 1$ equations, we obtain

$\bar{\theta} = 0$, $e_{ij} = (2\pi/n)$ $\forall i, j$ and the equivalent angular spacing ($t \to \infty$).

V. SIMULATION RESULTS AND ANALYSIS

To address the problem of multi-UAV cooperative tracking, we design control laws and demonstrate their validity. Simulation tests are performed for only the minimal persistent information architecture. The non-minimally persistent information architecture has the same properties, and thus, the analysis process does not include the associated results. In the simulation process, we study the tracking characteristics of four UAVs for stationary targets and two UAVs around moving targets.

A. THE INITIAL CONDITIONS

The initial conditions are as follows: $\mu_0 = 20\text{m}/s$, $r_d = 300m$, $\Delta V_{\max} = 5m/s$, $x_{10} = 500m$, $y_{10} = 500m$, $\psi_{10} = 0$, $x_{20} = -800m$, $y_{20} = -600m$, $\psi_{20} = \pi/2$, $x_{30} = -500m$, $y_{30} = 500m$, $\psi_{30} = \pi$, $x_{40} = 700m$, $y_{40} = -100m$ and $\psi_{10} = -\pi/4$.

B. SIMULATION RESULTS AND ANALYSIS

In Figs. 4 to 8, we present the simulation results with the initial conditions and assumptions described above. They are shown in the following:

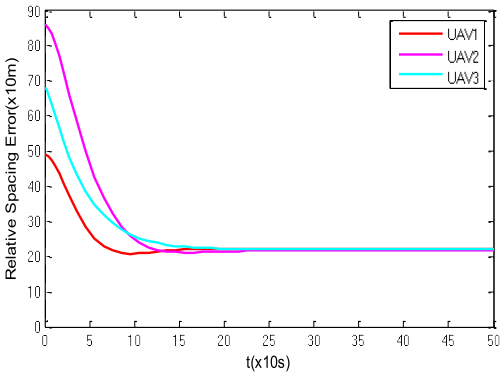

FIGURE 4. The relative distance between a UAV and stationary target.

Fig. 4 adopts the three-UAV formation as a control object and presents the relative distance error between the UAV and the target in the process of tracking a moving target, which shows a tendency to a level state after a rapid decline. As can be seen from Fig. 4, the UAV formation consists of one leader and two followers and is rapidly closing in on the target. From 1 s to 15 s, the leader of the formation is in front of the follower, and the forward velocity is larger than that of the two followers. Moreover, the geometric shape of the formation remains triangular but not congruent. After 15 s, the three UAVs are evenly distributed on a spherical surface whose center is the target and whose radius is the relative distance between them. They gradually become close to the target with the same attitude and position. The UAV tracks the target with the highest velocity and best optimized path before the UAV is close to the target; when the UAV is very close to the target, the UAV formation can achieve cooperative tracking with a fixed geometric shape.

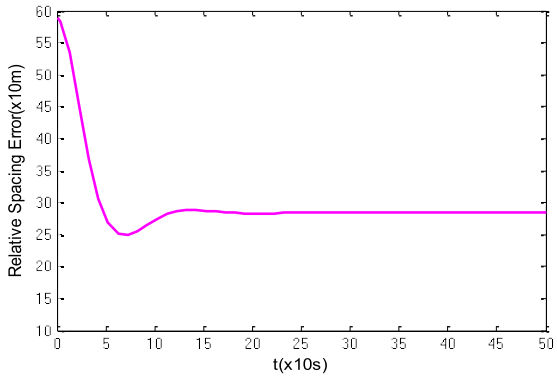

FIGURE 5. The relative distance error between two UAVs around the stationary target.

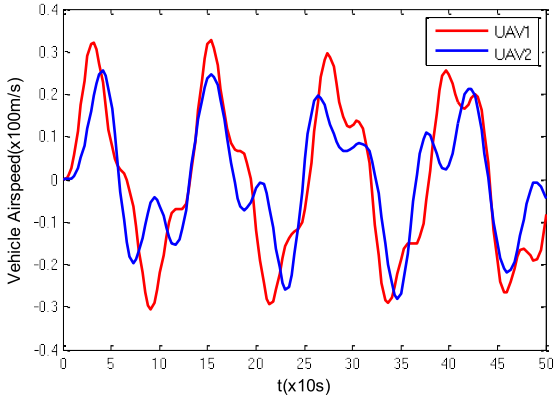

FIGURE 6. The airspeed command between the spacing and maintaining a circular orbit.

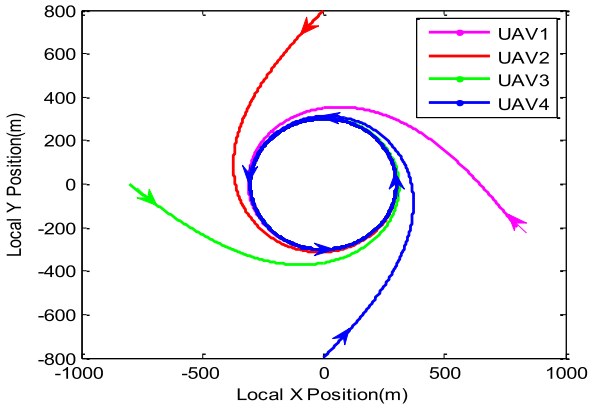

FIGURE 7. The four-UAV motion trajectories around the stationary target.

Figs. 5 and 6 adopt the two UAVs as a control object. Fig. 5 shows the relative distance error between two UAVs around a stationary target, which presents a tendency to decrease and then increase. When tracking the target with the shortest time, the multi-UAV formation will be affected by air

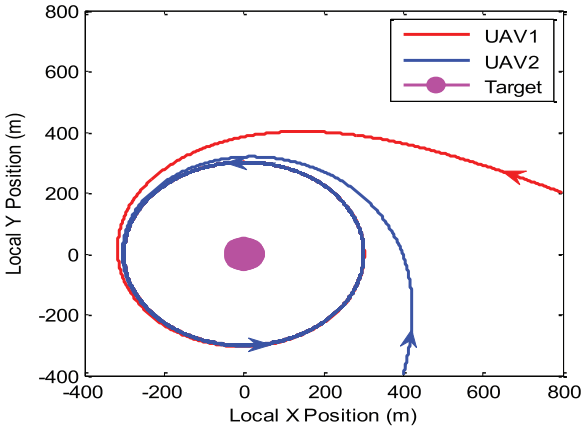

FIGURE 8. The two-UAV motion trajectory around the moving target.

resistance because the wingtip will generate a vortex effect. When the relative distance between two UAVs is appropriate, the air resistance will decrease, by which the velocity of the UAV formation will be improved. At 6.5 s, the vortex effect is the strongest, and simultaneously, the high-speed UAVs will generate a mutually repulsive effect. After 7 s, the relative distance error between two UAVs remains constant, and the UAV formation tracks the target under the triangular structure.

Fig. 6 presents the airspeed command between the spacing and maintaining a circular orbit around the moving target, and it shows a trend for cooperative formation flight; however, a delaying phenomenon is present. For the cooperative tracking controller process, each UAV is equipped with a control command sensor. In particular, there is a phenomenon whereby the received information is deviated during high-speed flight.

Fig. 7 shows the four UAVs' trajectories around the stationary target. Initially, the UAV has multiple headings and loiter circles, all of which converge to the desired heading along the Lyapunov guidance vector field. When all UAVs reach a loiter circular orbit with the prescribed distance, the variable airspeed controllers can achieve the desired angular spacing.

Fig. 8 shows the two UAV trajectories around the moving target. During the high-speed tracking of a moving target by the UAV formation, changes in the heading are always important in maintaining the UAV formation's shape. In addition, two UAVs gradually converge to the desired circular orbit with the designed control laws in the Lyapunov guidance field.

VI. CONCLUSION

To address the cooperative UAV formation tracking problem, we design control laws and prove the stability of tracking a moving target based on the Lyapunov guidance field through theoretical research. For the path planning of a single UAV, we present a proof of heading convergence to address the previously neglected timescale issue, and then, we propose a novel heading convergence method. We also analyze the guidance vector field using the analytical solution method, which provides an advantage for the combination of theory and practice. In the case of unknown wind and a moving target, we use the adaptive estimates to ensure the stability of the circular trajectory. For multi-UAV formations, the variable airspeed controller can achieve the desired spatial positions. Based on the control of a formation two UAVs, we establish the information architecture of UAV formation using rigid graph theory, which can achieve globally asymptotic stability. Meanwhile, a cloud-based data communication enables UAV generated heterogeneous data transmission.

This paper only studies one aspect of intelligent control; there are other potential research directions that can be studied. First, with increasing number of UAVs in the formation, the dynamic coupling effect between them becomes more complicated. Second, the adaptive control technology can expand to general moving targets. Further, this paper is only theoretical research and needs to be applied to actual engineering. Finally, the connection between the distributed control laws and the multi-UAV model is conducive to the study of more general UAV formation structures using graph theory. The design of the multi-UAV distributed control laws is one of the difficulties to be addressed and also the focus of the next step in our study. At present, the designed cooperative tracking controller is not embedded into the real UAV due to the limitation of conditions, the next major focus of our research will be to implement the designed controller in a practical application.

REFERENCES

[1] T. H. Summers, M. R. Akella, and M. J. Mears, "Coordinated standoff tracking of moving targets: Control laws and information architectures," *J. Guid. Control Dyn.*, vol. 32, no. 1, pp. 56–69, 2009.
[2] L. Gupta, R. Jain, and G. Vaszkun, "Survey of important issues in UAV communication networks," *IEEE Commun. Surveys Tuts.*, vol. 18, no. 2, pp. 1123–1152, 2nd Quart., 2016.
[3] X. Hu *et al.*, "Emotion-aware cognitive system in multi-channel cognitive radio ad hoc networks," *IEEE Commun. Mag.*, vol. 56, no. 4, pp. 180–187, Apr. 2018.
[4] X. Kong *et al.*, "Mobility dataset generation for vehicular social networks based on floating car data," *IEEE Trans. Veh. Technol.*, vol. 67, no. 5, pp. 3874–3886, May 2018.
[5] X. Hu, X. Li, E. Ngai, V. Leung, and P. Kruchten, "Multidimensional context-aware social network architecture for mobile crowdsensing," *IEEE Commun. Mag.*, vol. 52, no. 6, pp. 78–87, Jun. 2014.
[6] X. Hu, J. Zhao, B. C. Seet, V. C. M. Leung, T. H. S. Chu, and H. Chan, "S-Aframe: Agent-based multilayer framework with context-aware semantic service for vehicular social networks," *IEEE Trans. Emerg. Topics Comput.*, vol. 3, no. 1, pp. 44–63, Mar. 2015.
[7] Z. Ning, X. Wang, X. Kong, and W. Hou, "A social-aware group formation framework for information diffusion in narrowband Internet of Things," *IEEE Internet Things J.*, vol. 5, no. 3, pp. 1527–1538, Jun. 2018.
[8] J. Zhang *et al.*, "Energy-latency tradeoff for energy-aware offloading in mobile edge computing networks," *IEEE Internet Things J.*, vol. 5, no. 4, pp. 2633–2645, Aug. 2018.
[9] X. Kong, X. Song, F. Xia, H. Guo, J. Wang, and A. Tolba, "LoTAD: Long-term traffic anomaly detection based on crowdsourced bus trajectory data," *World Wide Web-Internet Web Inf. Syst.*, vol. 21, no. 3, pp. 825–847, May 2018.
[10] Y. Guo, X. Hu, B. Hu, J. Cheng, M. Zhou, and R. Y. K. Kwok, "Mobile cyber physical systems: Current challenges and future networking applications," *IEEE Access*, vol. 6, pp. 12360–12368, 2017.
[11] Z. Ning *et al.*, "A cooperative quality-aware service access system for social Internet of vehicles," *IEEE Internet Things J.*, vol. 5, no. 4, pp. 2506–2517, Aug. 2018.

[12] N. Zunli, Z. Xuejun, and G. Xiangmin, "UAV formation flight based on artificial potential force in 3D environment," in *Proc. Chin. Control Decis. Conf.*, May 2017, pp. 5465–5470.
[13] O. Cetin and G. Yilmaz, "Real-time autonomous UAV formation flight with collision and obstacle avoidance in unknown environment," *J. Intell. Robot. Syst.*, vol. 84, no. 4, pp. 415–433, Dec. 2016.
[14] F. Bullo, *Optimal Sensor Placement and Motion Coordination for Target Tracking*. New York, NY, USA: Pergamon, 2006.
[15] K. Abu-Jbara, W. Alheadary, G. Sundaramorthi, and C. Claudel, "A robust vision-based runway detection and tracking algorithm for automatic UAV landing," *Int. Conf. Unmanned Aircr. Syst.*, Jun. 2015, pp. 1148–1157.
[16] D. Kingston and R. Beard, "UAV splay state configuration for moving targets in wind," in *Advances in Cooperative Control and Optimization*. Berlin, Germany: Springer, 2007, pp. 109–128.
[17] H. Liu, M. Cao, and C. W. Wu, "Coupling strength allocation for synchronization in complex networks using spectral graph theory," *IEEE Trans. Circuits Syst. I, Reg. Papers*, vol. 61, no. 5, pp. 1520–1530, May 2017.
[18] E. W. Frew, D. A. Lawrence, and S. Morris, "Coordinated standoff tracking of moving targets using Lyapunov guidance vector fields," *J. Guid. Control Dyn.*, vol. 31, no. 2, pp. 290–306, 2008.
[19] J. A. Marshall, M. E. Broucke, and B. A. Francis, *Pursuit Formations of Unicycles*. New York, NY, USA: Pergamon, 2006.
[20] K. Savla, F. Bullo, and E. Frazzoli, "On traveling salesperson problems for Dubins' vehicle: Stochastic and dynamic environments," in *Proc. IEEE Conf. Decis. Control*, Dec. 2005, pp. 4530–4535.
[21] S. Griffiths, "Vector field approach for curved path following for miniature aerial vehicles," in *Proc. AIAA Guid., Navigat., Control Conf. Exhib.*, 2006, pp. 1–15.
[22] T. Eren, P. N. Belhumeur, B. D. O. Anderson, and A. S. Morse, "A framework for maintaining formations based on rigidity," *IFAC Proc.*, vol. 35, no. 1, pp. 499–504, 2002.
[23] J. Baillieul and A. Suri, "Information patterns and Hedging Brockett's theorem in controlling vehicle formations," in *Proc. IEEE Conf. Decis. Control*, Dec. 2003, pp. 556–563.
[24] B. D. O. Anderson, P. N. Belhumeur, T. Eren, A. S. Morse, and W. Whiteley, "Operations on rigid formations of autonomous agents," *Commun. Inf. Syst.*, vol. 3, no. 4, pp. 223–258, 2004.
[25] C. Yu *et al.*, "Three and higher dimensional autonomous formations: Rigidity, persistence and structural persistence," *Automatica*, vol. 43, no. 3, pp. 387–402, Mar. 2007.
[26] B. Fidan, C. Yu, and B. D. O. Anderson, "Acquiring and maintaining persistence of autonomous multi-vehicle formations," *IET Control Theory Appl.*, vol. 1, no. 2, pp. 452–460, Mar. 2007.
[27] L. Henneberg, *Die graphische Statik der starren Systeme*. Sonnewalde, Germany: B. G. Teubner, 1911.
[28] C. Godsil and G. F. Royle, *Algebraic Graph Theory*. Springer, 2001.
[29] Z. Xiandi and L. Zhengliang, *Graph Theory and Its Application*. Beijing, China: Higher Education Press, 2005.
[30] G. F. Royle and C. Godsil, *Algebraic Graph Theory*. New York, NY, USA: Springer, 2001, pp. 55–58.

JIALONG ZHANG received the B.Eng. degree from the North China Institute of Aerospace Engineering in 2014, and the M.E. degree from the College of Aeronautics and Astronautics Engineering, Air Force Engineering University, in 2017. He is currently pursuing the Ph.D. degree with the School of Automation, Northwestern Polytechnical University. His main research interests lies in cooperative UAV formation flight control.

JIANGUO YAN received the B.Eng. degree from the College of Astronautics Engineering, National University of Defense Technology, in 1983, and the Ph.D. degree from the School of Automation Control, Northwestern Polytechnical University, in 2007. His research interests include computer control and intelligent control, pattern recognition, robust control, navigation, guidance and flight control, and optical flight control.

PU ZHANG received the B.Eng. and M.Eng. degrees from the North China Institute of Aerospace Engineering in 2008 and 2012, respectively. She is currently pursuing the Ph.D. degree with Northwestern Polytechnical University. Her main research interests lie in management and optimization.

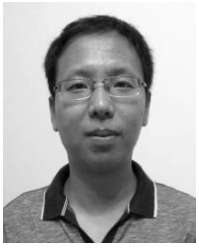

XIANGJIE KONG received the B.Eng. degree from the College of Information Science and Engineering, Zhejiang University, Hangzhou, China, in 2004, and the Ph.D. degree from the School of Software, Dalian University of technology, Dalian, China, in 2009. He is currently an Associate Professor with the School of Software, Dalian University of technology, Dalian. His interests lie in big data, mobile computing, and computational social science.